LIP-STUDENTS-24-13

Calibration of the Scintillator Detectors from the Pierre Auger Observatory

Diogo Vilaça[1,a], Mariana Macedo[1,b] , and Miguel Lacerda[1,c]

[1] *Universidade do Minho, Braga, Portugal*

Project supervisor: Raul Sarmento

September 21, 2024

Abstract. The objective of this project was the measurement of the calibration constant for the new scintillator detectors installed in the Pierre Auger Observatory, using data from a testing tank with a hodoscope of *Resistive Plate Chambers*. First, the data from that tank was analyzed, studying the different detectors, the measured events and how to filter the data only to retrieve events of muons. In the process, small variations in the muon hump charge were discovered. These were incompatible with the statistical error bars, and a study was conducted to trace the cause of such variations, up to no avail. An initial calibration constant was computed, obtaining 1.19 with a good fit. Due to the reduced common area in the detectors, an extrapolation was done using a Monte Carlo simulation, obtaining a new calibration constant of 1.20 with an estimated uncertainty of 10 %.

Keywords: Pierre Auger Observatory, Calibration, Detector, Scintillator, C++, ROOT

1 Introduction

The Pierre Auger Observatory is the largest observatory of particle showers in the world. Located in Pampa Amarilla, Argentina, this observatory is a hybrid detector, which employs two independent methods to detect and study the high energy particle showers. One of those methods detects the particles through their interaction with the water inside the surface detection tanks (via the production of Cherenkov light) [1][2][3].

There are 1661 water-Cherenkov detectors spaced by 1.5 km (and 750 m) in a triangular grid. Each of them has 10 m^2 of surface and a height of 1.2 m. Their interior has three photomultipliers and walls covered by a reflective material. This enables the simultaneous measurement of the muonic and electromagnetic components of the particle showers.

When the photomultipliers (PMTs) receive Cherenkov light emitted by a particle that crosses the tank, they generate an electric current (in ADC units, from *analog-to-digital*). To have a physical meaning, this charge is converted (calibrated), to units equivalent to the equivalent charge of a centered vertical muon (VEM).

This project's objective is to measure the calibration constant of the new scintillators (SSD - *Scintillator Surface Detector*) installed on top of the tanks, using a hodoscope of *Resistive Plate Chambers* (RPCs) mounted on the testing tank, which consists of two segmented plane detectors, one on the top of the tank and SSD and the other on the bottom of the tank. This setup can be observed in Figure 1[4].

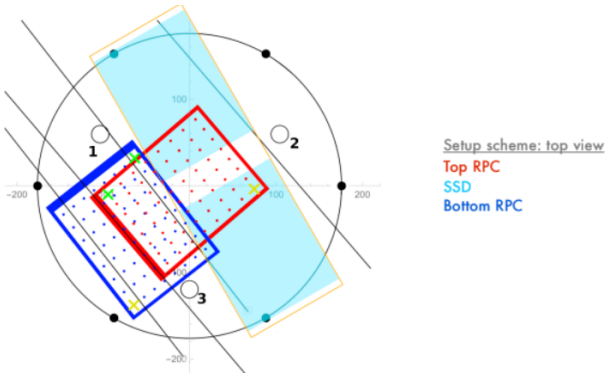

Figure 1. Setup scheme of the testing tank[4].

The formula for the calibration constant is in Equation 1, where Q_{MHC} is the average muon hump charge (in ADC), that is, the average charge of the omnidirectional muons (they can have any trajectory), and Q_{MIP} is the charge of the vertical muons (in ADC/VMIP). Thus, the calibration constant is the ratio between the maxima of these curves. This calibration constant formula is similar to the one used to calibrate the PMTs[5].

$$S = \frac{Q_{MHC}}{Q_{MIP}} \tag{1}$$

2 Analysis of the Data From the Observatory

The Pierre Auger Observatory provided the data measured by the detectors in the testing tank, from 17:00 until 9:00 of the next day. This data was analyzed to understand better the detected events and how to filter the data needed to obtain the calibration constant.

2.1 Analysis of the Events in the Cherenkov Tank

The first step was to analyze the total number of events triggered by the RPC hodoscope during the respective pe-

[a] e-mail: dioze2323@gmail.com
[b] e-mail: marianamacedo.vm@gmail.com
[c] e-mail: miguellacerda6268@gmail.com

riod (the histogram "Total events" in Figure 2), as well as the events corresponding only to the passage of a single muon through the RPCs (the histogram "Single hit events" in Figure 2).

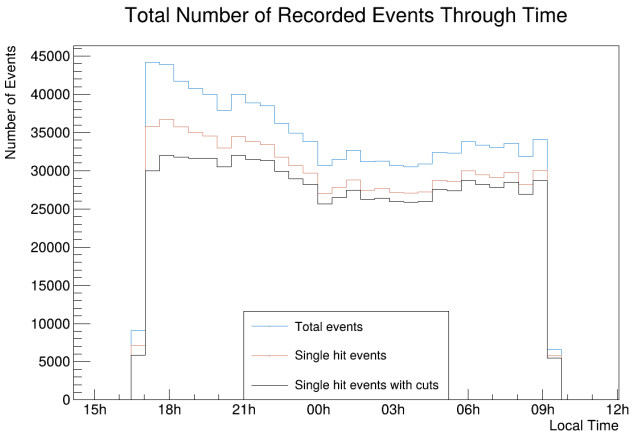

Figure 2. Histogram of the total events triggered by the hodoscope ("Total events"), as well as the single hit events ("Single hit events") and the single hit and single peak events ("Single hit events with cuts").

In Figure 2, the histogram "Single hit events with cuts" corresponds to the number of events that are both single hit (only on muon detected by the RPCs) and single peak (only one muon detected by the PMTs).

There's a significant difference between the total number of events and the number of single hit and single peak events from 17:00 to, approximately, 22:00. This could be due to thermal noise in the RPCs since the temperature is higher at this time interval than the rest of the measuring period.

Following this, the data of the different types of events for each PMT was analyzed, removing those who aren't single hits. The obtained results are very similar between the PMTs. The histograms for each event type for PMT 1 can be found in Figure 3.

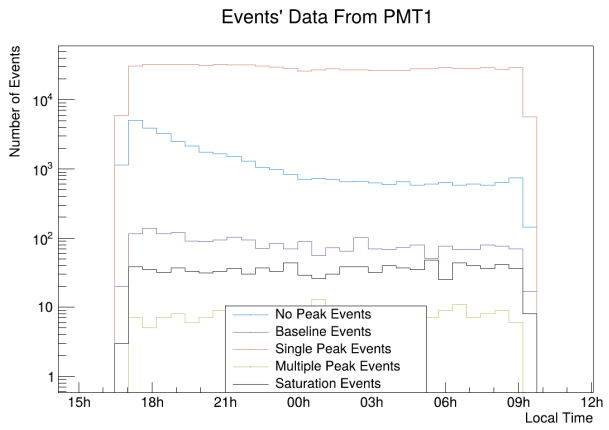

Figure 3. Histogram of the number of events, in logarithmic scale, for each type of event measured in PMT1.

In Figure 3:

- "No peak events" correspond to events occurring in the RPCs where nothing is detected in the Cherenkov tank. This mostly corresponds to noise effects in the RPCs.
- "Baseline events" are events for which the signal is not at the expected position, instead it is at where the baseline is calculated.
- "Multiple peak events" are events in which more than one muon is detected simultaneously in the tank. This could be due to muons that cross the tank without crossing the RPCs.
- "Saturation events" are events in which the photomultipliers saturate, i.e. the Cherenkov light received is such that the device reaches the maximum measurable current. It can occur in muon showers.

There is a greater predominance of "No peak events" between 17:00 and 22:00, decreasing over time. This corroborates the hypothesis that thermal noise affects RPCs, mentioned earlier.

2.2 Analysis of the Scintillator's Events

After analyzing the events in the test tank, the analysis of the events in the scintillator (SSD) began, starting with the analysis of the total number of events and filtering the data in the previous manner. The results can be found in Figure 4, where "Total events" is the total number of events total events triggered by the hodoscope, "SSD Total events" are the total number of events measured by the SSD, "SSD total events w/ cuts" are the number of events measured in the SSD that are both single peak and single hit and "SSD Single hit events" are the number of events measured by the SSD that are single hit events.

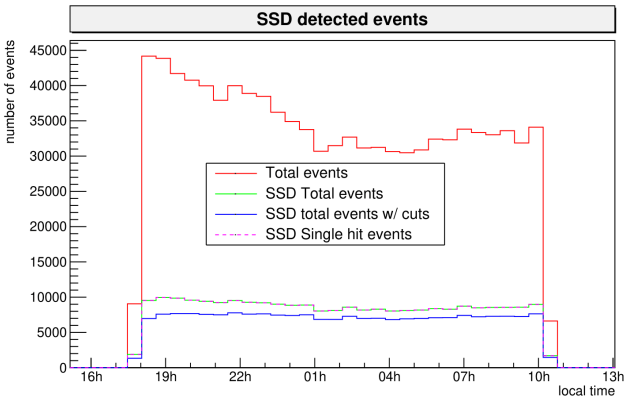

Figure 4. Histogram of the number of events in the SSD ("SSD Total events"), in comparison with the total number of events measured in the testing tank ("Total events") and the single hit events ("SSD Single hit events") and the single hit and single peak events ("SSD total events w/ cuts").

The total number of events measured by the SSD is approximately equal to the number of single-hit events measured by the SSD, showed by the overlapping histograms

in Figure 4. Thus, a great part of the SSD's data can be used to calibrate this device. There's also a great difference between the total number of events detected by the SSD and those detected by the tank since only a small fraction crosses the SSD, inferable by analyzing the geometry of the setup in Figure 1.

Similarly to section 2.1, the data of the different types of events for the SSD was analyzed, whose results can be found in Figure 5.

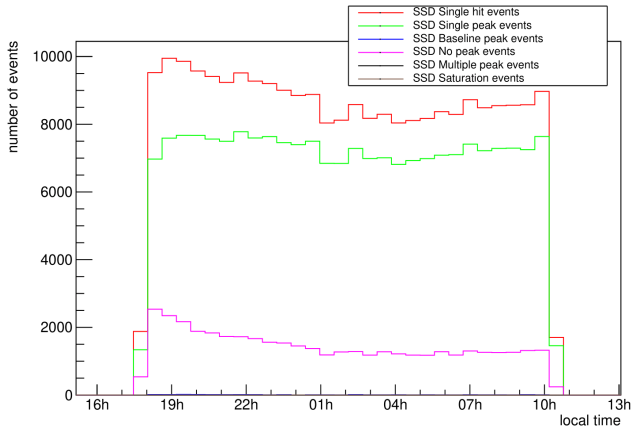

Figure 5. Histogram of the number of events for each type of event measured in the SSD.

It can be concluded that the vast majority are single peak events, followed by no peak events (which are most likely noise events, similar to the PMTs' case). There is also the same thermal noise effect seen with the PMTs. In the SSD, there are no saturation events, baseline events nor multiple peak events.

2.3 Analysis of the Charge's Distribution

To better understand the type of phenomena whose information is collected by the PMTs, histograms of the charge distribution at different scales have been constructed. Since the results are similar to every PMT, only the results for PMT1 are shown in Figure 6.

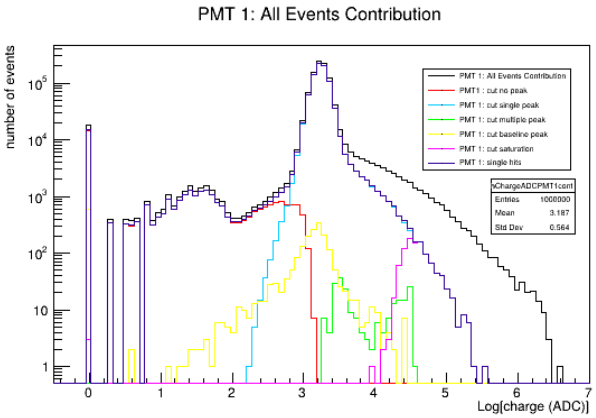

Figure 6. Histogram of the logarithm of the charge distribution (in ADC) for each event type measured in PMT1.

Initially, there were histograms constructed of the number of events according to their charge up to a maximum of 10 000 ADC. The PMTs' histograms were very similar, allowing the same conclusions to be drawn from them. However, there were no charge distributions for the saturation events. For this reason, histograms of the logarithm of the charge were created with a higher upper charge limit, which showed the saturation events, between 20 000 ADC and 50 000 ADC.

The no peak events correspond to noise events, with charges of less than 1000 ADC.

After examining the information collected from the photomultipliers, it's important to do the same for the scintillator, so that they can be compared. The same steps previously mentioned were followed, and the results can be found in Figure 7.

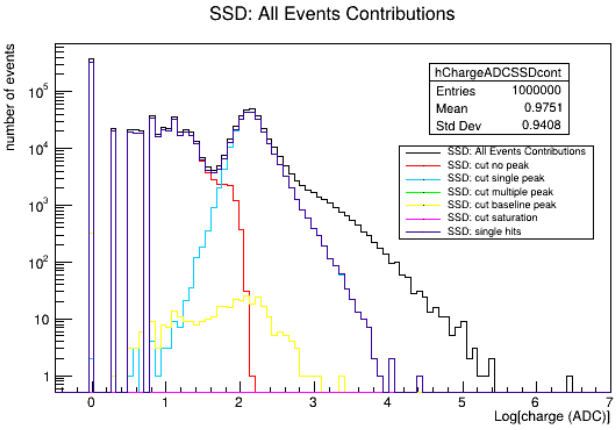

Figure 7. Histogram of the logarithm of the charge distribution (in ADC) for each event type measured in the SSD.

Saturation events and multiple peak events are absent. As these are rare events and the probability of a muon hitting the SSD and passing through the tank is small, the probability of this happening for two or more muons simultaneously is much lower.

The baseline peak events have lower charges in the SSD than in the PMTs, where most events have a charge equal to 1000 ADC.

2.4 Analysis of the PMTs' Calibrated Charge

The calibrated charge of the PMTs over time was also analyzed, as shown in Figure 8.

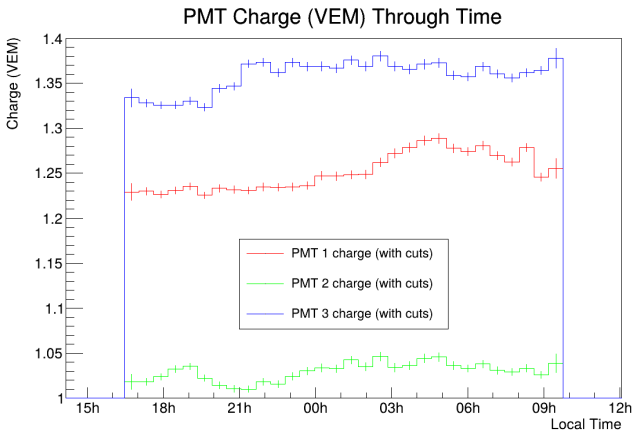

Figure 8. Graph of the PMTs' calibrated charge (in VEM) through time for the single hit and single peak events.

Removing all the undesired events, i.e. considering only the single hit and single peak events, there are still small variations incompatible with the statistical error bars, which isn't expected for the calibrated charge.

Two main hypotheses were proposed:

- these variations are influenced by a change in the predominant trajectory of the muons, which could affect the amount of emitted Cherenkov light.
- these changes could be the effect of some electronic instability in the PMTs.

3 Analysis of the Variation of the Calibrated Charge

3.1 Analysis of the Muons' Trajectories Through the RPCs

To begin studying the hypothesis that the predominant trajectories influence the variation in the calibrated charge, the number of events for each RPCs pads was analyzed and represented in 2D histograms. The 2D histograms with the total number of events for the top and bottom RPCs are in Figures 9 and 10, respectively. The data is shown in a representation similar to the geometry of the RPC. Figures 11 and 12 show the same data for the top RPC and the bottom RPC, respectively, but through time.

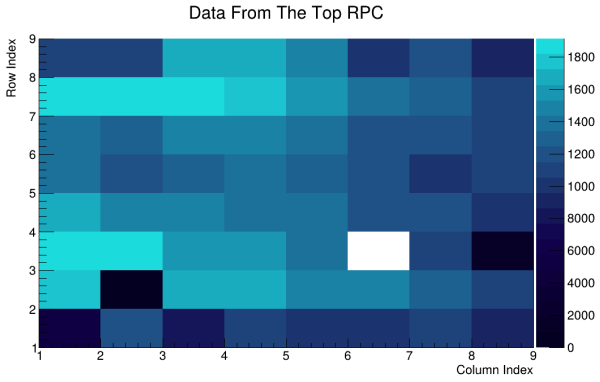

Figure 9. Total number of single hit and single peak events per pad in the top RPC.

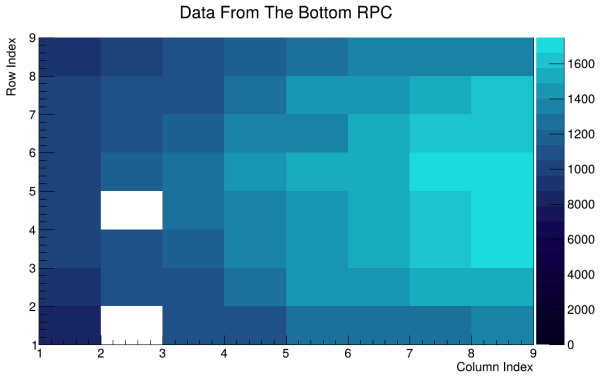

Figure 10. Total number of single hit and single peak events per pad in the bottom RPC.

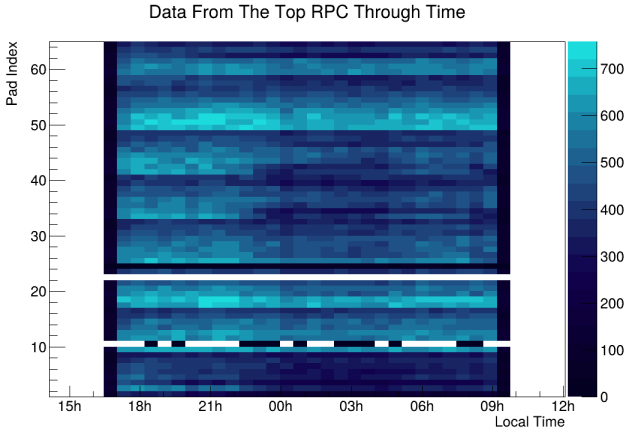

Figure 11. Total number of single hit and single peak events per pad through time for the top RPC.

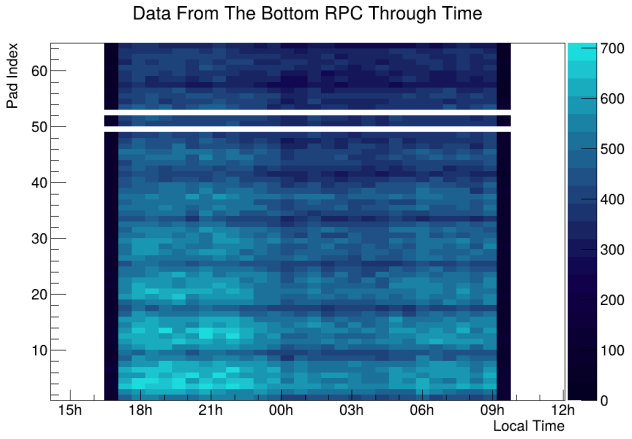

Figure 12. Total number of single hit and single peak events per pad through time for the bottom RPC.

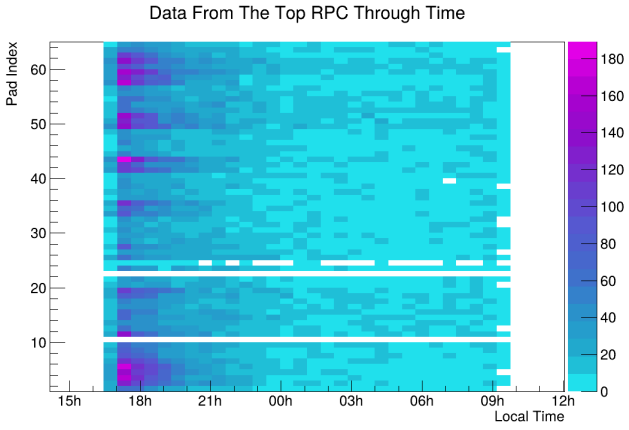

Figure 13. Total number of no peak events (noise) per pad through time for the top RPC.

The higher incidence of events in certain parts of the RPCs (the regions with a higher number of events than the neighbors in Figures 9 and 10) is due to their geometry and the distribution of muon trajectories.

There are three non-functional pads in the top RPC, and two non-functional pads in the bottom RPC, because either data is missing for these pads, or the number of events for them is close to zero.

There is a time effect in a region of the top RPC (a spot on Figure 11) from 22:00 onwards. In this period there is a region with fewer muon events.

As the spot is not uniform for all pads, the temperature change may not fully explain the spot, as each pad in an RPC should have approximately the same temperature.

3.2 Noise Analysis in the RPCs

A possible explanation for the variation in the top RPCs pattern is that this RPC is above the tank, so it is more exposed to factors that can induce noise. With this hypothesis in mind, the effect of noise was studied along the pads of each RPC (the no peak events). The histogram with the total number of no peak events in the top and bottom RPCs through time can be found in Figure 13 and 14, respectively.

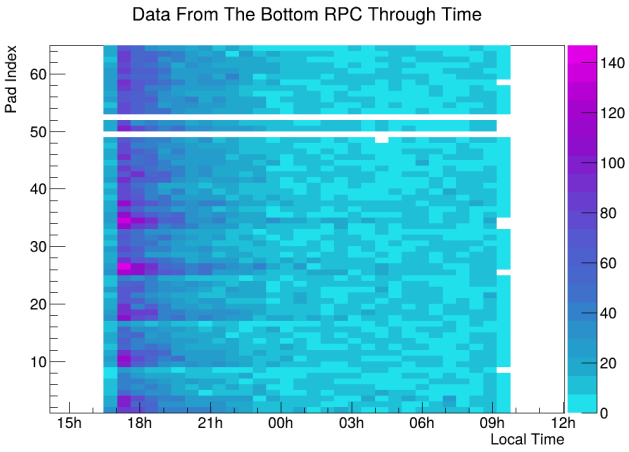

Figure 14. Total number of no peak events (noise) per pad through time for the bottom RPC.

In the spots observed in the previous section, the noise is approximately uniform, which can be seen in Figure 13, which leads to the conclusion that this variation is not influenced by noise.

3.3 Analysis of the Muons' Trajectories' Angles and the Traveled Distances

The previous results led to the analysis of the event detection angles and the distance traveled by the muons in the tank. The effect of filtering the data using the separate PMT data or on the joint data of the three PMTs was also analyzed. The graph for the average zenith and average azimuthal angles through time can be found in Figures 15 and 16, respectively.

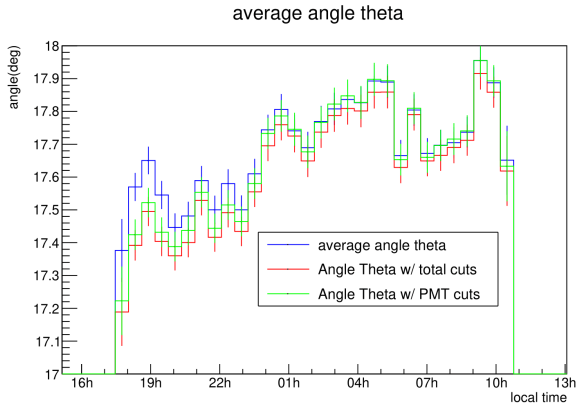

Figure 15. Average zenith angle for the muons' trajectories through time, for the total number of events ("average angle theta"), for the single peak and single hit events using the separate PMTs' data ("Angle Theta w/ total cuts") and for the single peak and single hit events using the joint PMTs' data ("Angle Theta w/ PMT cuts").

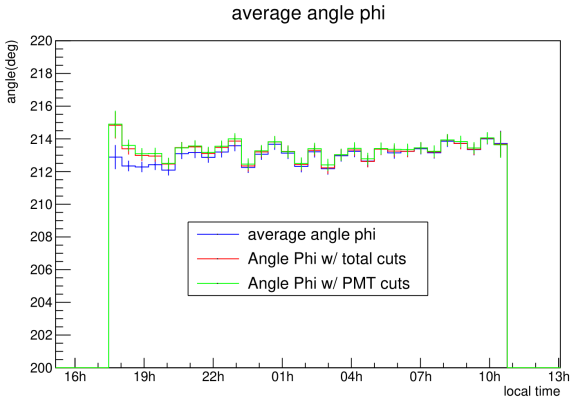

Figure 16. Average azimuthal angle for the muons' trajectories through time, for the total number of events ("average angle phi"), for the single peak and single hit events using the separate PMTs' data ("Angle Phi w/ total cuts") and for the single peak and single hit events using the joint PMTs' data ("Angle Phi w/ PMT cuts").

It can be observed that there is not much difference between using the joint PMT data or using the individual PMTs' data, since both histograms are within each other's error bars.

There is a noticeable variation in the zenith angle at night, but it's less than 1 % of the average. Both angle variations are less than 1 % compared to the average value. So the angles' variation does not explain the variation in the calibrated charge, which is about 3 % to 4 %.

3.4 Analysis of the Normalized Calibrated Charge

All the previous analyses led to the creation of the graph of the normalized calibrated charge, i.e. the division of the calibrated charge by the distance traveled by the muons, which is shown in Figure 17. If the variation is due to the traveled distance, the graph will be approximately constant, since the greater the traveled distance, the greater the amount of Cherenkov light produced, and the greater the charge.

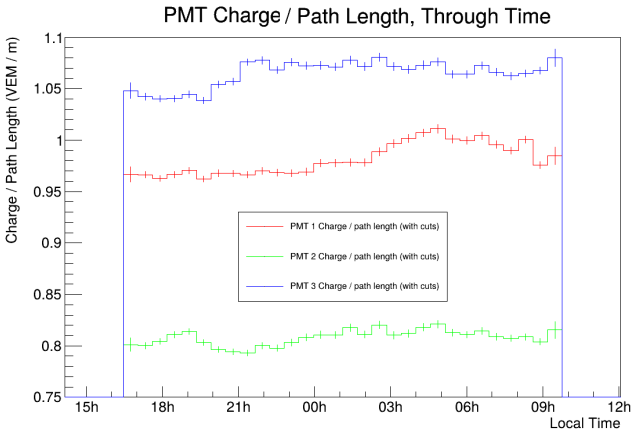

Figure 17. Graph of the PMTs' calibrated normalized charge (in VEM per meter) through time for the single hit and single peak events.

The graph shows that the variations in the calibrated charge remain the same, which are not explained by the statistical error bars. Therefore, the variation is not caused by the distance traveled by the muons.

3.5 Study of the Relative Percent Difference

Finally, the last hypothesis was that the effect of the variation arises from some variable used in the calculation of the calibrated charge itself (similar to Equation 1), mainly in the muon hump charge. To test this, the graphs of the relative percentage difference (relating to the average value) of the muon hump charge (in Figure 19), the ADC charge (in Figure 18), and the calibrated charges (in Figure 20) were plotted, for the PMTS.

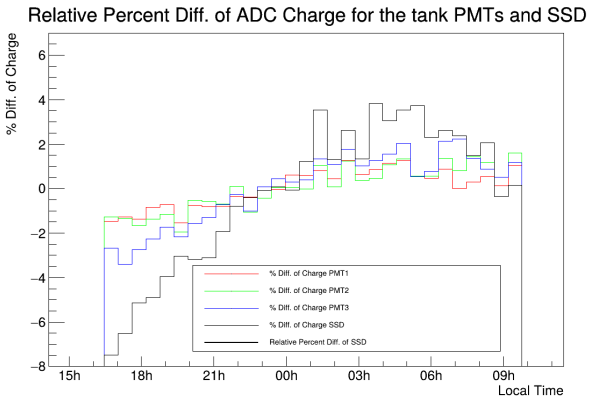

Figure 18. Graph of the percent difference relating to the average value of the ADC charge through time, for each PMT and the SSD.

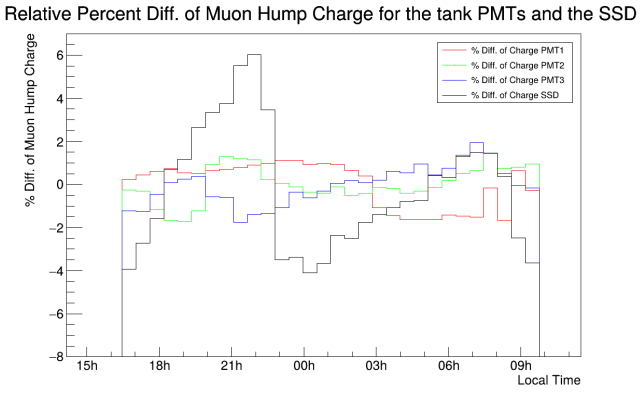

Figure 19. Graph of the percent difference relating to the average value of the muon hump charge through time, for each PMT and the SSD.

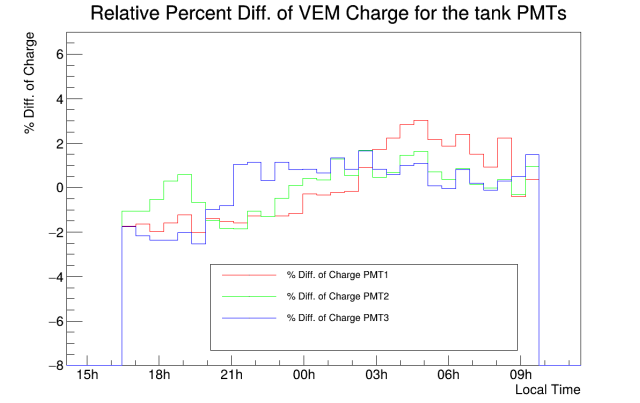

Figure 20. Graph of the percent difference relating to the average value of the calibrated charge through time, for each PMT.

It should be noted that the absolute value of the ADC charge is meaningless; the values vary depending on the environmental conditions, hence the need for a calibrated charge.

The PMTs have similar behaviors for the ADC charge. There seems to be no clear relationship between variations in ADC charge and temporal variations in VEM charge.

The problem lies in the muon hump charge. There are temporal instabilities in its time evolution which result in temporal variations in the average value of the charge calibrated in VEM. The origin of these PMT instabilities should be investigated in detail in the future.

4 Scintillator's Calibration Constant

4.1 Obtaining the Vertical Muons

To obtain only the charge of the vertical muons, in addition to the data filtering used previously, an extra condition was applied which restricts the distance traveled by the muons to differ by a maximum of 1 % of the tank's height, i.e. the distance traveled must be between 1.2 m and 1.212 m. The effect of this filtering can be seen by comparing the number of events in the SSD before applying the extra condition, in Figure 21, and after applying the extra condition, in Figure 22.

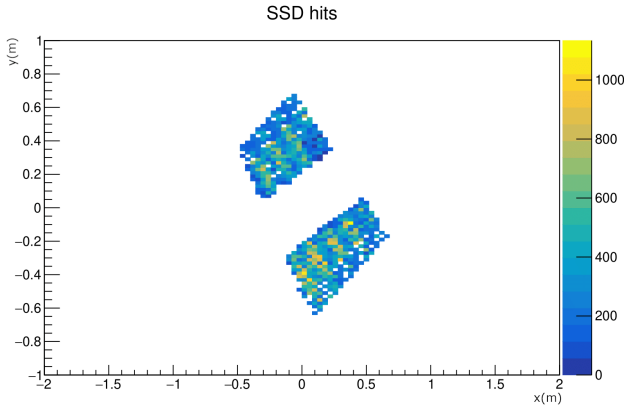

Figure 21. 2D histogram of the number of events in the SSD applying the data filtering used in the previous sections.

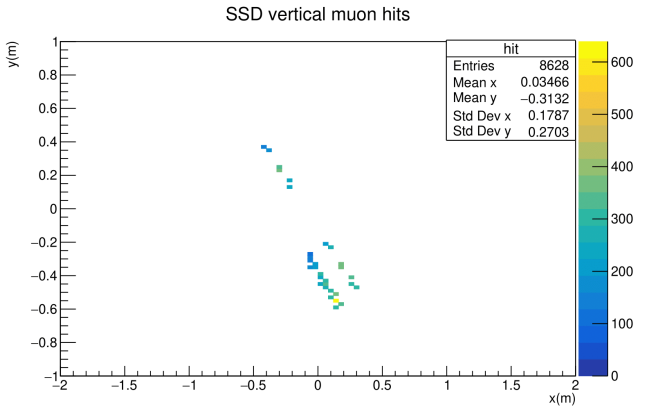

Figure 22. 2D histogram of the number of events in the SSD applying the data filtering used in the previous sections plus the extra condition to ensure only the vertical muons.

4.2 Calibration Constant

Two fits were made to the maximum of the scintillator's ADC vertical MIP charge histogram, a second-order polynomial fit, and a Gaussian fit. It was found that both adjustments obtain maxima within the error range. Therefore, either adjustment can be used. The Gaussian fit was chosen. The graph with the ADC charge distribution, as well as its fits and the muon hump charge distribution, can be found in Figure 23.

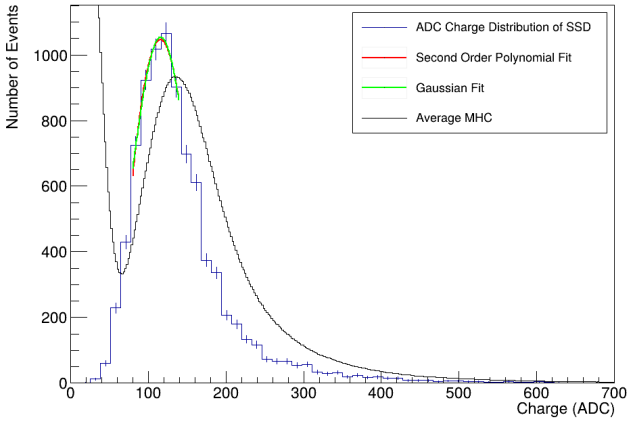

Figure 23. Graph with the muon hump charge distribution for the muons, the ADC charge distribution, and its two fits (one Gaussian and the other second-degree polynomial) for the vertical muons.

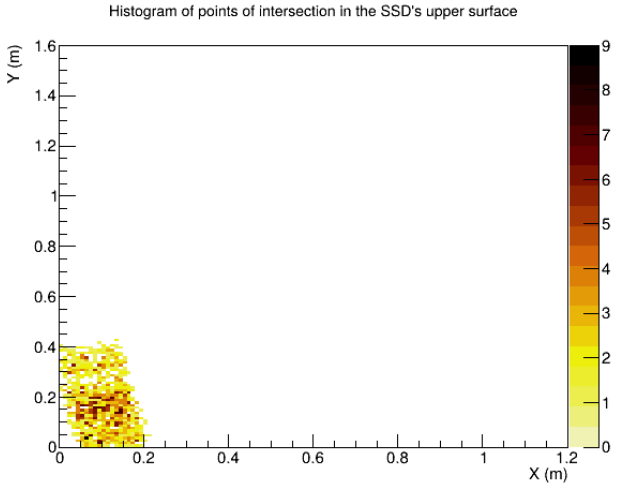

Figure 24. 2D histogram of the number of simulated events in the scintillator for the upper surface.

Using Equation 1, this resulted in a calibration constant of approximately 1.19, with a Chi-square/NDF value of 0.71, a good quality fit.

However, the data from the vertical muons only corresponds to a small part of the scintillator, as this is the small area in common with the RPCs and the vertical MIP charge in the scintillator is not uniform[1]. To obtain a calibration constant more adequate to the entire scintillator, the result will have to be extrapolated to the rest of the scintillator.

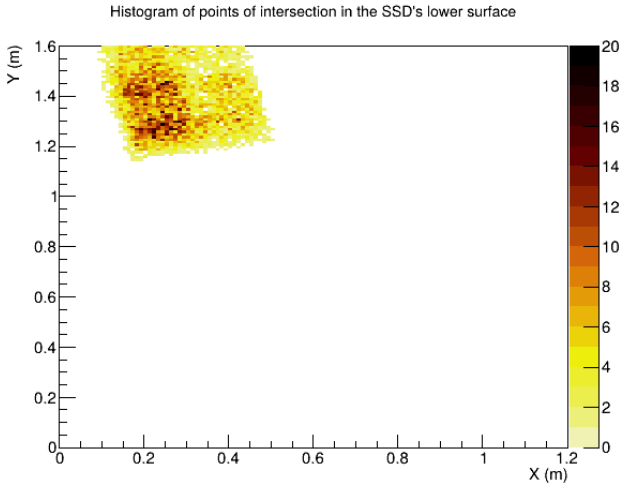

Figure 25. 2D histogram of the number of simulated events in the scintillator for the lower surface.

5 Extrapolation of the Calibration Constant

To carry out the extrapolation, a Monte Carlo simulation was performed to generate random points on the pads of the RPCs that had vertical muon events. This is because the pads have a non-negligible area, and detection implies that the muon may have passed through one of several possible points in this area. The results obtained from this simulation are in Figures 24 and 25.

The data of the charge along the scintillator was obtained from a study carried out at the Karlsruhe Institute of Technology[1].

These were in PDF format, so to extract the data from the graph, the online tool "2D Reader"[6] had to be used.

The intersection of the trajectory of the simulated muons in the scintillator was calculated and the weighted average of the charge in the scintillator was calculated, in the cells where it was hit by muons, using the number of muons that hit that cell as the weight. The arithmetic average of the charge in the points of intersection was also computed.

The corrected calibration constant is given by Equation 2, where S_0 is the original calibration constant, $\bar{Q}_W$ is the VMIP charge's weighted average on the scintillator and $\bar{Q}_A$ is the average VMIP charge in those points.

$$S = S_0 \frac{\bar{Q}_W}{\bar{Q}_A} \quad (2)$$

Using Equation 2, the new calibration constant is 1.20 with an estimated uncertainty of 10 %.

6 Results and Conclusions

After analyzing and filtering the data from the testing tank and performing an extrapolation on it, the measured calibration constant for the scintillator is 1.20 with an estimated uncertainty of 10 %, thus achieving the project's objective.

Due to the limited time for the execution of this project, not every task was completed, as such, there is work to be done in the future, for example, a more detailed study of the cause of the variation of the muon hump charge, as well as the systematic computation of the errors associated with the final calibration constant.

This work consists of a big step for the observatory, which will help to better detect different particle events, while never losing sight of the hypothesis of discovering and measuring new physics.

Acknowledgments

We appreciate LIP for giving us the opportunity to work on this project during the summer internship and providing us with the necessary resources. We also appreciate the Pierre Augier Observatory for this project and for supplying the necessary support.

Lastly, we greatly appreciate our supervisor Raul Sarmento, for all the indispensably useful guidance during the project, crucial to its success.

References

[1] T.P.A. Collaboration, Science Reviews - from the end of the world **1**, 8–33 (2020)

[2] P.A. Observatory, *The pierre auger observatory*, https://www.auger.org/observatory/

[3] LIP, *The Pierre Auger Observatory*, https://pages.lip.pt/auger/the-pierre-auger-observatory/

[4] G. Franco, Master's thesis, Centro Brasileiro de Pesquisas Físicas (2023)

[5] T.P.A. Collaboration, Nuclear Instruments and Methods in Physics Research Section A: Accelerators, Spectrometers, Detectors and Associated Equipment **798**, 172 (2015)

[6] *2D Reader - graphreader.com*, https://www.graphreader.com/2dreader, accessed: 29-07-2024